# Imaging in reflecting spheres

Cite as: Chaos 32, 093136 (2022); doi: 10.1063/5.0110865
Submitted: 17 July 2022 · Accepted: 29 August 2022 ·
Published Online: 26 September 2022



Jean-Pierre Eckmann,[1] Gemunu H. Gunaratne,[2,a)] Jason Shulman,[2,3] and Lowell T. Wood[2]

## AFFILIATIONS

[1]Département de Physique Théorique and Section de Mathématiques, Université de Genève, 1211 Geneva 4, Switzerland
[2]Department of Physics, University of Houston, Houston, Texas 77204, USA
[3]Department of Physics, Stockton University, Galloway, New Jersey 08205, USA

[a)]**Author to whom correspondence should be addressed:** gemunu@uh.edu

## ABSTRACT

We study the formation of images in a reflective sphere in three configurations using caustics on the field of light rays. The optical wavefront emerging from a source point reaching a subject following passage through the optical system is, in general, a Gaussian surface with partial focus along the two principal directions of the Gaussian surface; i.e., there are two images of the source point, each with partial focus. As the source point moves, the images move on two surfaces, referred to as *viewable surfaces*. In our systems, one viewable surface consists of points with radial focus and the other consists of points with azimuthal focus. The problems we study are (1) imaging of a parallel beam of light, (2) imaging of the infinite viewed from a location outside the sphere, and (3) imaging of a planar object viewed through the point of its intersection with the radial line normal to the plane. We verify the existence of two images experimentally and show that the distance between them agrees with the computations.



**The locations of optical images are typically calculated using ray diagrams or by maximizing the flux density of rays. Recent studies have emphasized that images form at caustics on the field of rays emerging from a source, i.e., where a finite energy is concentrated. In general, following passage through an optical system, a wavefront entering a point of observation does not appear to emerge from a single focus, but rather has partial focus at two points, which only coincide in highly symmetric configurations. The two resulting image surfaces can be found by computing caustics on the field of rays. We implement these computations for reflections from a sphere in three distinct configurations. The results for one of them are tested in an experiment.**

## I. INTRODUCTION

In an as yet unpublished treatise on visual perception (Feigenbaum, unpublished), the late chaos-theorist M. J. Feigenbaum discussed formation of images in optical systems, which form at caustics of the field of light rays (Born and Wolf, 1965; Shealy, 1976; Nussenzveig, 1977; Nye, 1999; Berry, 2015; and Berry, 2021). Specifically, a small section of a spherical wavefront emerging from an object will evolve during its passage through an optical system to a Gaussian surface characterized by two orthogonal principal directions and the associated radii. Partial focusing of rays is only achieved along these principal directions as illustrated in Fig. 1 (Kinsler, 1945; Bartlett *et al.*, 1984; Horváth *et al.*, 2003; and Eckmann, 2021). The wavefront can be represented using the two families of rays (here chosen to be vertical and horizontal) appearing to emerge from a pair of distinct "non-objects" $V$ and $H$. On focusing at $V$, the horizontal direction will appear unfocused, the view being referred to as *horizontal astigmatism*. Similarly, focusing on $H$, the vertical direction will appear unfocused, resulting in *vertical astigmatism*. Although the visual system is capable of focusing on either image, Feigenbaum argued that it naturally selects the vertically astigmatic image. However, unlike prior conjectures (Horváth *et al.*, 2003), he showed that this choice is not predicated on binocularity by requesting subjects to report what is seen with one eye closed.

Feigenbaum (unpublished) illustrates the formation of a particular class of *anamorphic* images, i.e., images formed in a cylindrical reflector of a horizontal table. One of the two images of the table was shown to lie inside the cylinder, while the other lay on the table behind the cylinder. The two surfaces on which the table was imaged were referred to as *viewable surfaces*. The viewable surface inside the cylinder consisted of points with horizontal focus (such as $H$), while that on the table behind the mirror contained points

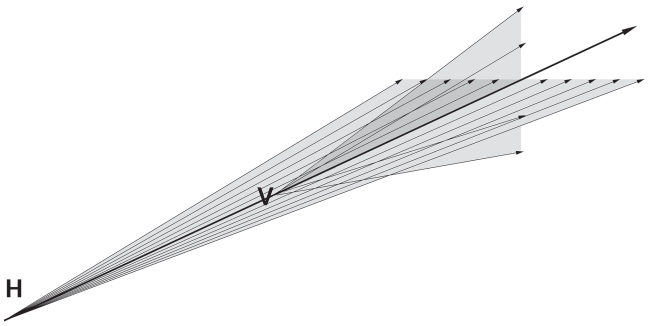


**FIG. 1.** An optical wavefront is a Gaussian surface defined by two principal directions and the associated radii. The only partial focus of rays is along these principal directions. The two families of rays appear to emerge from "images" at *H* and *V*. Reproduced with permission from J.-P. Eckmann, Am. J. Phys. **89**, 955–962 (2021). Copyright 2021 AIP Publishing LLC (Eckmann, 2021).

with vertical focus (such as *V*). As predicted, it was found that in erect viewing, subjects observe the image within the mirror, while in orthogonal viewing (with eyes parallel to the mirror axis), they observe the image on the table.

In this paper, we study imaging from a "witch ball," i.e., a reflective sphere. Viewing through the sphere, one observes a deformed image of its surroundings. This phenomenon is well-known and, for example, discussed in Berry (1972, 2015) where one of the images is calculated. Here, we extend the study using the approach of Feigenbaum (unpublished). These findings involve calculation of caustics (Born and Wolf, 1965; Shealy, 1976; and Avendaño Alejo, 2013), which are simple geometry, albeit somewhat tedious.

The calculation outlined in Sec. II is that of locating images of a parallel beam of light impinging on the sphere. One image surface consists of points of radial focus. It is an azimuthally symmetric surface whose cross section contains a cusp singularity. The calculation is that presented in Berry (2015). The second surface consists of points of azimuthal focus. Symmetry considerations dictate that the surface is degenerate, collapsing to the mirror axis parallel to the incoming beam.

In Sec. III, we consider a configuration where both viewable surfaces are non-degenerate. It is the viewpoint of a cycloptic (i.e., single-eyed) observer at a finite distance viewing the infinite through the sphere. Two distinct surfaces are found *inside* the sphere, distinguished by different types of astigmatism, radial and azimuthal. It is found that if the viewing distance is approximately 3.73 times the radius of the sphere, the radially focused viewing surface is planar to fourth order in perturbation. It is an ideal distance to capture a photographic image of the infinite viewed in the sphere.

A second non-degenerate problem considered in Sec. IV consists of viewing a plane through the point of intersection of a mirror axis with the plane. Once again, we find two image surfaces associated with radial and azimuthal astigmatism. In Sec. V, we demonstrate the presence of two distinct images and compare experimentally measured inter-image distances with results from the computation.

Section VI discusses implications of our results.

## II. IMAGES OF A PARALLEL INCOMING BEAM

Studies outlined in this section refer to the configuration shown schematically in Fig. 2(a). A beam of light, incident in the $-\hat{\mathbf{z}}$-direction, impinges on and reflects off the sphere. A representative ray reflects from a point on the witch ball defined by polar angles $(\theta, \phi)$, $\theta$ being the angle of incidence. The direction of the incident ray $\hat{\mathbf{t}}_i$ and the normal $\hat{\mathbf{n}}$ to the sphere at incidence are

$$\hat{\mathbf{t}}_i = [\underline{0},\ -1], \quad \hat{\mathbf{n}} = [\sin\theta\ \underline{e^{i\phi}},\ \cos\theta],$$

where the underbar in the complex first component indicates that the $\hat{\mathbf{x}}$ and $\hat{\mathbf{y}}$ components are the real and imaginary parts of the complex number. In this representation, the scalar product of two vectors $\left[u_1\underline{e^{i\phi_1}}, z_1\right]$ and $\left[u_2\underline{e^{i\phi_2}}, z_2\right]$ is $u_1u_2\cos(\phi_1-\phi_2)+z_1z_2$.

Define a second basis $\{\hat{\mathbf{x}}', \hat{\mathbf{y}}', \hat{\mathbf{z}}'\}$ such that $\hat{\mathbf{z}}' \equiv \hat{\mathbf{z}}$ and the plane of reflection is the $\hat{\mathbf{x}}'\hat{\mathbf{z}}'$ plane as shown in Fig. 2. The new basis vectors are

$$\hat{\mathbf{x}}' = \left[\underline{e^{i\phi}}, 0\right]; \quad \hat{\mathbf{y}}' = \left[\underline{i\,e^{i\phi}}, 0\right]; \quad \hat{\mathbf{z}}' = \left[\underline{0}, 1\right]. \tag{1}$$

Reflection of the ray in the $\hat{\mathbf{x}}'\hat{\mathbf{z}}'$ plane is shown in Fig. 2(b). The outgoing ray begins at the point of incidence $\mathbf{e}_0 = \hat{\mathbf{n}}$ and is directed

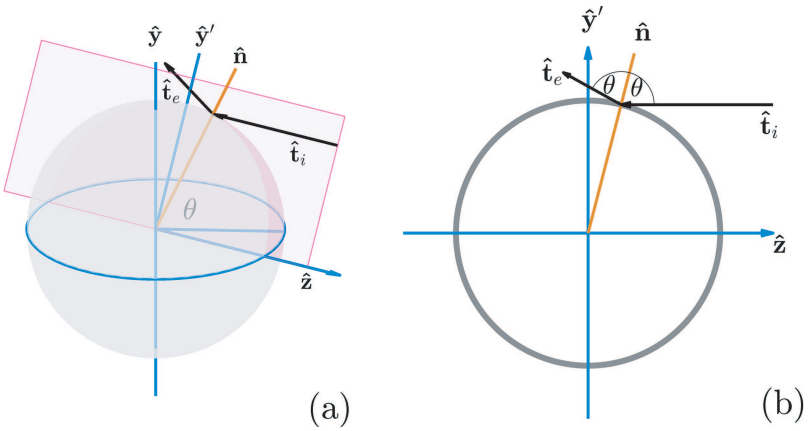


**FIG. 2.** (a) A schematic of a ray of light (black), incident along the $\mathbf{t}_i = -\hat{\mathbf{z}}$ direction, impinging on a spherical witch ball of radius $R = 1$. The ray is incident on and reflects from the surface at the point defined by polar angles $(\theta, \phi)$. (b) The ray diagram in the plane $(\mathbf{t}_i,\ \hat{\mathbf{n}})$.

along

$$\hat{\mathbf{t}}_e = \sin 2\theta\, \hat{\mathbf{x}}' + \cos 2\theta\, \hat{\mathbf{z}}' = \left[\sin 2\theta\, \underline{e^{i\phi}},\ \cos 2\theta\right].$$

Hence, the outgoing ray can be parameterized as

$$\mathbf{r}(s;\theta,\phi) = \mathbf{e}_0 + s\cdot\hat{\mathbf{t}}_e = \left[(\sin\theta + s\sin 2\theta)\,\underline{e^{i\phi}},\ \cos\theta + s\cos 2\theta\right], \tag{2}$$

where the parameter $s$ is the distance of a point on the exit ray from the point of reflection.

In Feigenbaum (unpublished), it is highlighted that images are formed on caustic surfaces of a wavefront and can be computed using a collection of neighboring exiting rays. The caustics, envelopes of neighboring rays, are given by $d\mathbf{r}(s) = 0$ (Shealy, 1976); i.e.,

$$\frac{\partial}{\partial\theta}\mathbf{r}(s;\theta,\phi)\,d\theta + \frac{\partial}{\partial\phi}\mathbf{r}(s;\theta,\phi)\,d\phi + \frac{\partial}{\partial s}\mathbf{r}(s;\theta,\phi)\,ds = 0. \tag{3}$$

Since the configuration is axially symmetric, we can select a cone of rays around $\phi = \pi/2$ (i.e., on the vertical axis) to evaluate the images. Using (2),

$$d\mathbf{r} = \left[(\cos\theta + 2s\cos 2\theta)\,\underline{i},\ -\sin\theta - 2s\sin 2\theta\right]d\theta + \left[-(\sin\theta + s\sin 2\theta)\,\underline{1},\ 0\right]d\phi + \left[\sin 2\theta\,\underline{i},\ \cos 2\theta\right]ds = 0, \tag{4}$$

whose $\hat{\mathbf{y}}$ and $\hat{\mathbf{z}}$ components are

$$(\cos\theta + 2s\cos 2\theta)\,d\theta + \sin 2\theta\, ds = 0,$$
$$-(\sin\theta + 2s\sin 2\theta)\,d\theta + \cos 2\theta\, ds = 0.$$

Setting the determinant of coefficients to zero gives

$$(\cos\theta + 2s)\ d\theta = 0. \tag{5}$$

The $\hat{\mathbf{x}}$ component of (4) is

$$(\sin\theta + s\sin 2\theta)\ d\phi = 0. \tag{6}$$

Equations (5) and (6) can be used to calculate locations of the images at $\phi = \pi/2$.

One solution to Eqs. (5) and (6) satisfies $d\phi = 0$ implying $d\theta \neq 0$ (for otherwise, we only have a single ray), and $s = s_R = -\frac{1}{2}\cos\theta$. The location of this image is

$$\mathbf{r}_R = \left[\left(\frac{3}{2}\cos\theta - \cos^3\theta\right)\underline{i},\ \sin^3\theta\right]. \tag{7}$$

The resulting surface, which we refer to as the $R$-caustic, consists of points of radial focus and azimuthal astigmatism. It is shown in red in Fig. 3 and contains a singularity on the $z$ axis. To establish the nature of the singularity, note that $y_R - 1/2 \sim \theta^2$ and $z_R \sim \theta^3$, and hence, the singularity is of power 3/2, i.e., a cusp singularity. This caustic is discussed in Berry (2015).

The second solution is given by $d\theta = 0$ and $d\phi \neq 0$. From (6), the value of $s$ for this image is $s_A = -\frac{1}{2\cos\theta}$, and the location of the image [from (2)] is

$$\mathbf{r}_A = \left[\underline{0},\ \frac{1}{2\cos\theta}\right] = \frac{1}{2\cos\theta}\,\hat{\mathbf{z}}. \tag{8}$$

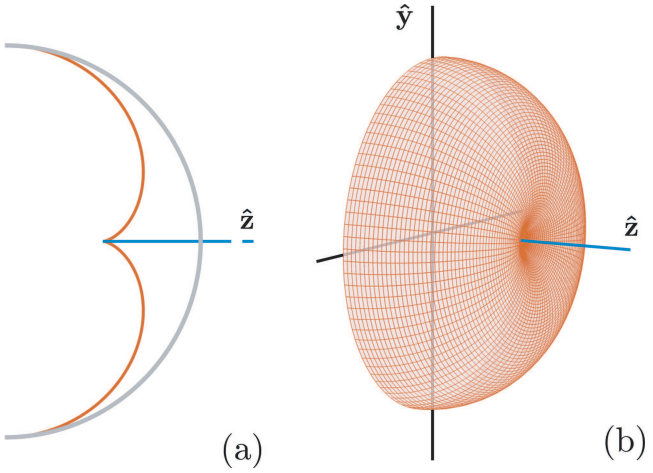


**FIG. 3.** The two caustics for reflection of a beam of light parallel to the $z$ axis from a spherical mirror. (a) The $R$-caustic, consisting of points from which radial fans of rays (appear to) emerge, is the cross section of the surface shown in red in (b). The cross section of the mirror is shown in gray. The blue line shows the degenerate $A$-caustic $[\frac{1}{2}, \infty)$ on the $z$ axis.

The surface containing points of azimuthal focus (and radial astigmatism) is called the $A$-caustic; it lies on the $\mathbf{z}$ axis at distances $[\frac{1}{2}, \infty)$ and is shown in blue in Fig. 3.

The degeneracy of the $A$-caustic originates from the azimuthal symmetry of the configuration. This is most easily deduced by noting that the exit ray reflected from a point defined by angles $(\theta, \phi)$ lies in the plane defined by $\phi$. Hence, two rays impinging at $\phi$ and $\phi + d\phi$ will meet on the intersection of the associated planes, which is the $z$ axis.

Note that one caustic was given by $d\phi = 0$. This was required by reflection symmetry of the configuration about the $y$ axis. Since the two caustics are orthogonal, the second is required to satisfy $d\theta = 0$. We will use these symmetry requirements to simplify computations in Secs. III and IV.

## III. VIEWING THE INFINITE THROUGH THE WITCH BALL

Consider cycloptic viewing of the witch ball from a point $O$ at a distance $D$ from its center, assumed without loss of generality to be on the $z$ axis. Points imaged are infinitely far away from the witch ball. Consider a ray of light arriving in a direction $\hat{\mathbf{t}}_i$ at the point $\hat{\mathbf{n}} = \left[\sin\theta\,\underline{e^{i\phi}},\ \cos\theta\right]$, on the mirror, and reflecting in a direction $\hat{\mathbf{t}}_e$ to reach the point $O = \left[\underline{0}, D\right]$. We search for images seen from $O$ of all infinitely far-away points.

Note first that, by the laws of reflection and time-reversal symmetry (i.e., $\hat{\mathbf{t}}_i \to -\hat{\mathbf{t}}_e$; $\hat{\mathbf{t}}_e \to -\hat{\mathbf{t}}_i$), the unit vectors $\hat{\mathbf{t}}_i$, $\hat{\mathbf{t}}_e$, and $\hat{\mathbf{n}}$ along a ray of incidence, ray of reflection, and the surface normal satisfy

$$\hat{\mathbf{t}}_e = -2(\hat{\mathbf{n}}\cdot\hat{\mathbf{t}}_i)\hat{\mathbf{n}} + \hat{\mathbf{t}}_i; \quad \hat{\mathbf{t}}_i = -2(\hat{\mathbf{n}}\cdot\hat{\mathbf{t}}_e)\hat{\mathbf{n}} + \hat{\mathbf{t}}_e. \tag{9}$$

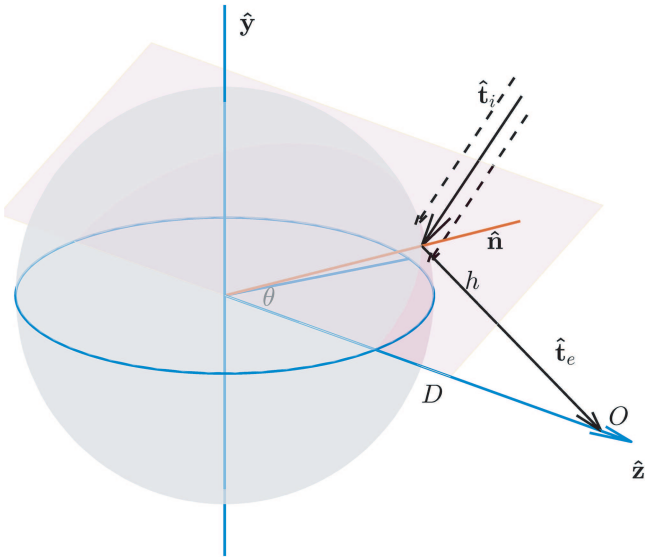


**FIG. 4.** The ray diagram for a beam arriving in a direction $\hat{\mathbf{t}}_i$ to the point $\hat{\mathbf{n}}$, on the mirror, and reflecting in a direction $\mathbf{t}_e$ to reach $O = [0, D]$. It is also necessary to follow reflections of a collection of rays parallel to $\hat{\mathbf{t}}_i$ that are incident on points near $\hat{\mathbf{n}}$.

For the configuration shown in Fig. 4,

$$\hat{\mathbf{n}} = \left[\sin\theta\ \underline{e^{i\phi}},\ \cos\theta\right],$$

$$\hat{\mathbf{t}}_e = \frac{1}{h}\left[-\sin\theta\ \underline{e^{i\phi}}, D - \cos\theta\right],$$

$$h = \sqrt{D^2 + 1 - 2D\cos\theta}.$$

It follows from (9) that

$$\hat{\mathbf{t}}_i = \frac{1}{h}\left[(\sin\theta - D\sin 2\theta)\ \underline{e^{i\phi}},\ (\cos\theta - D\cos 2\theta)\right].$$

[It can be verified that $\hat{\mathbf{t}}_e = -2(\hat{\mathbf{n}}\cdot\hat{\mathbf{t}}_i)\hat{\mathbf{n}} + \hat{\mathbf{t}}_i$.]

What is to be performed is a calculation of the image formed by a beam of rays parallel to $\hat{\mathbf{t}}_i$ that impinges on the sphere in the neighborhood of $\hat{\mathbf{n}}$. Toward this end, consider such a ray incident on the mirror at a point defined by angles $(\theta + \mu)$ and $(\phi + \nu)$ for small $\mu$ and $\nu$. The normal at its point of incidence is

$$\hat{\mathbf{n}}' = \left[\sin(\theta+\mu)\ \underline{e^{i(\phi+\nu)}},\ \cos(\theta+\mu)\right],$$

and the ray reflects in a direction $\hat{\mathbf{t}}'_e = -2(\hat{\mathbf{n}}'\cdot\hat{\mathbf{t}}_i)\hat{\mathbf{n}}' + \hat{\mathbf{t}}_i$.

As the incident direction changes, the contact with the caustic slides along the caustic, with potential jumps from one smooth section to another one, for example, from the top red arc to the bottom red arc in Fig. 3. The surface containing all such points is referred to as the "viewable surface" in Feigenbaum (unpublished). Notice that viewable surfaces depend both on the caustic and the objects viewed. Below, we compute these surfaces associated with the $R$- and $A$-caustics. Due to azimuthal symmetry, the images for only a single value of $\phi$, selected to be $\phi = \pi/2$, need to be calculated.

### A. The *R*-viewable surface

The $R$-viewable surface consists of locations of radial focus of far-away points and satisfies $\nu = 0$. With $\phi = \pi/2$, we find $\hat{\mathbf{n}}' = \left[\sin(\theta+\mu)\ \underline{i},\ \cos(\theta+\mu)\right]$, and consequently,

$$\hat{\mathbf{n}}'\cdot\hat{\mathbf{t}}_i = \frac{1}{h}\left\{\cos\mu - D\cos(\theta-\mu)\right\}.$$

From (9), we get

$$\hat{\mathbf{t}}'_e = -2(\hat{\mathbf{n}}'\cdot\hat{\mathbf{t}}_i)\left[\sin(\theta+\mu)\ \underline{i},\ \cos(\theta+\mu)\right] + \frac{1}{h}\left[(\sin\theta - D\sin 2\theta)\ \underline{i},\ (\cos\theta - D\cos 2\theta)\right].$$

The exit ray is $\mathbf{r}_R(\mu, t) = \hat{\mathbf{n}}' + s\cdot\hat{\mathbf{t}}'_e$, and the $R$-viewable surface is given by

$$d\mathbf{r}' = \left(\frac{\partial\mathbf{r}'}{\partial\mu}\right)_{\mu=0} d\mu + \left(\frac{\partial\mathbf{r}'}{\partial s}\right)_{\mu=0} ds = 0.$$

Noting that

$$\left(\frac{\partial\hat{\mathbf{n}}'}{\partial\mu}\right)_{\mu=0} = \left[\cos\theta\ \underline{i}, -\sin\theta\right],$$

$$\hat{\mathbf{t}}'_e|_{\mu=0} = \frac{1}{h}\left[-\sin\theta\ \underline{i}, (D-\cos\theta)\right],$$

$$\left(\frac{\partial\hat{\mathbf{t}}'_e}{\partial\mu}\right)_{\mu=0} = \frac{2}{h}\left[(D-\cos\theta)\ \underline{i},\ \sin\theta\right],$$

we find that the $x$-projection is identically satisfied, while the $y$- and $z$-projections give

$$\left\{\cos\theta + \frac{2s}{h}(D-\cos\theta)\right\} d\mu - \frac{\sin\theta}{h} ds = 0,$$

$$-\left(1 - \frac{2s}{h}\right)\sin\theta\, d\mu + \frac{(D-\cos\theta)}{h} ds = 0.$$

Consistency of the pair of equations yields

$$s_R = -\frac{1}{2}\frac{(D\cos\theta - 1)}{h},$$

whereupon the location of the image is found to be

$$\mathbf{r}_R = \hat{\mathbf{n}} + s_R\cdot\hat{\mathbf{t}}_e = \left[\sin\theta\left(1 - \frac{(D-\cos\theta)}{h^2}\right)\underline{i},\ \cos\theta - \frac{(D\cos\theta - 1)(D-\cos\theta)}{2h^2}\right]. \tag{10}$$

Figure 5 shows cross sections of the caustic surface for $D = 1.5R$, $D = 3.73R$, and $D = 20R$. Note that the surface is nearly flat for the intermediate configuration, as seen from Fig. 5, and is, therefore, an extremely good surface for sharp imaging.

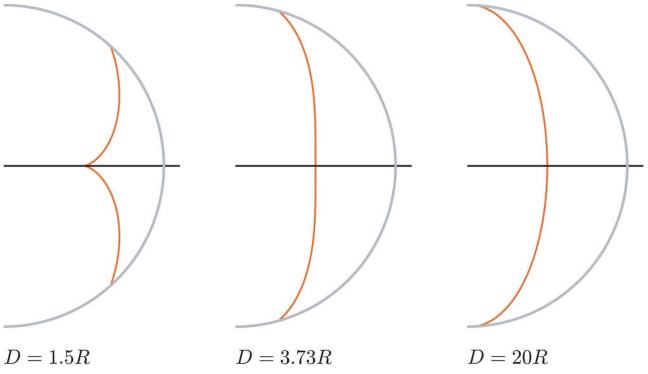


**FIG. 5.** Cross sections of the *R*-caustics for three values of the viewing distance *D*.

The shape of the viewable surface near the axis of symmetry is

$$\left(z_R - \frac{1}{2}\right) = \frac{1}{2}\left(\frac{D}{(D-1)^2} - \frac{1}{2}\right)\theta^2 + \mathcal{O}(\theta^4);$$
$$y_R = \frac{(D-2)}{(D-1)}\theta + \mathcal{O}(\theta^2),$$

showing that the surface $z_R = z_R(y_R)$ is quadratic except when $D = 2 + \sqrt{3} \approx 3.73$ when it is quartic.

### B. The *A*-viewable surface

The *A*-viewable surface consists of locations of azimuthal focus satisfying $\mu = 0$. With $\phi = \pi/2$, we find $\hat{\mathbf{n}}' = \left[\sin\theta\ \underline{\mathrm{i}}\,\mathrm{e}^{\mathrm{i}\nu},\ \cos\theta\right]$, and consequently,

$$\hat{\mathbf{n}}' \cdot \hat{\mathbf{t}}_i = \frac{1}{h}\left\{(1 - D\cos\theta) + (\cos\nu - 1)\Gamma\right\},$$

where $\Gamma = \sin\theta(\sin\theta - D\sin 2\theta)$. From (9),

$$\hat{\mathbf{t}}'_e = -2(\hat{\mathbf{n}}' \cdot \hat{\mathbf{t}}_i)\left[\sin\theta\ \underline{\mathrm{i}}\,\mathrm{e}^{\mathrm{i}\nu},\ \cos\theta\right] + \frac{1}{h}\left[(\sin\theta - D\sin 2\theta)\ \underline{\mathrm{i}},\ (\cos\theta - D\cos 2\theta)\right].$$

The exit ray is $\mathbf{r}_A(\mu, t) = \hat{\mathbf{n}}' + s \cdot \hat{\mathbf{t}}'_e$, and setting $\nu = 0$, the *A*-viewable surface is given by

$$0 = \mathrm{d}\mathbf{r}'_A = \left\{\left[-\sin\theta\ \underline{1},\ 0\right] - 2s(\hat{\mathbf{n}}' \cdot \hat{\mathbf{t}}_i)\left[-\sin\theta\ \underline{1},\ 0\right]\right\} \times \mathrm{d}\nu\left\{-2(\hat{\mathbf{n}}' \cdot \hat{\mathbf{t}}_i)\left[\sin\theta\ \underline{\mathrm{i}},\ \cos\theta\right] + \frac{1}{h}\left[(\sin\theta - D\sin 2\theta) \times \underline{\mathrm{i}},\ (\cos\theta - D\cos 2\theta)\right]\right\}\mathrm{d}s.$$

Projecting in the *y*-direction gives $\mathrm{d}s = 0$, and projecting in the *x*-direction gives

$$s_A = -\frac{1}{2}\frac{h}{(D\cos\theta - 1)}.$$

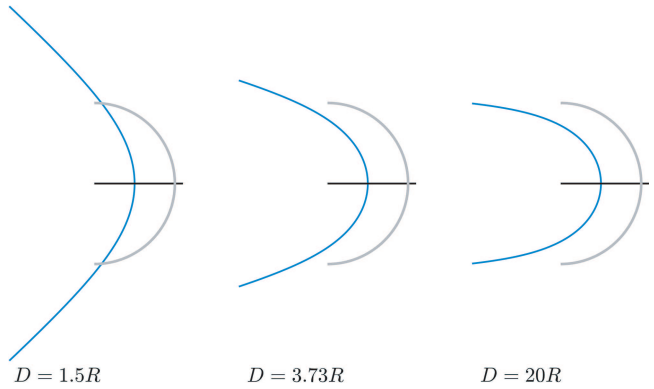


**FIG. 6.** Cross sections of *A*-viewable surfaces for three values of the viewing distance *D*.

The location of the image is

$$\mathbf{r}_A = \hat{\mathbf{n}} + s_A \cdot \hat{\mathbf{t}}_e = \left[\left\{\sin\theta + \frac{\sin\theta}{2(D\cos\theta - 1)}\right\}\underline{\mathrm{i}}, \cos\theta - \frac{(D - \cos\theta)}{2(D\cos\theta - 1)}\right].$$

For the *A*-viewable surface, $z_A = 1/2 + \mathcal{O}(y_A^2)$ at the symmetry axis, where the quadratic term is a function of *D* that does not vanish at any *D*.

The *z*-coordinate of the viewable surface moves to $-\infty$ as the incoming ray reaches grazing incidence at $\theta = \sin^{-1}(1/D)$. Figure 6 shows cross sections of the viewable surface for $D = 1.5R$, $D = 3.73R$, and $D = 20R$.

## IV. VIEWING A PLANAR SURFACE FROM ITS CENTER

Figure 7 shows another configuration with non-degenerate viewable surfaces. An image, such as a photograph, lies on the yellow plane (shown in projection) a distance *D* from the center of the mirror. The observer places the eye at the intersection of the black dashed line (looking to the left through a small hole in the center of the yellow surface). The reflected image can then be seen in two different locations depending on the astigmatism. In Fig. 8, the cross section of the *R*-viewable surface is shown in red and that of the *A*-viewable surface in blue. At the edges, focus will be at different depths.

The path of a representative ray from a point $P = \left[y_0\mathrm{i},\ D\right]$ on the photograph to the observation point *O* is shown in Fig. 7. Note that since the configuration is axially symmetric, we have, without loss of generality, chosen $\phi = \pi/2$. The direction of the incoming ray is

$$\hat{\mathbf{t}}_i = \frac{1}{h_i}\left[(\sin\theta - y_0)\ \underline{\mathrm{i}},\ (\cos\theta - D)\right],$$

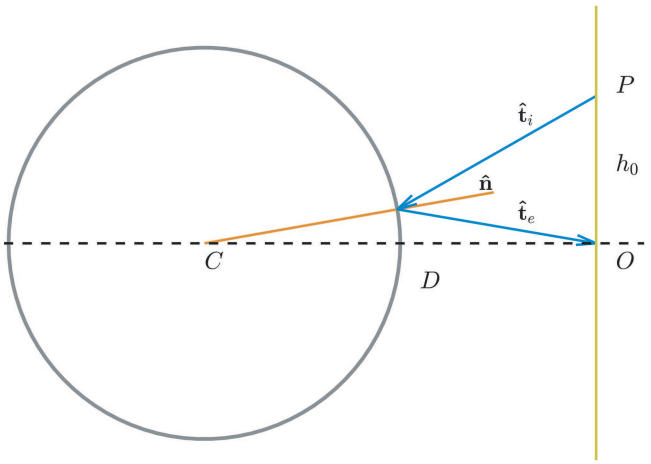


**FIG. 7.** Viewing an image of a plane (yellow) in the witch ball. The image is viewed from *O* and the intersection of the plane with the diameter normal to it. The ray from *P* reaches *O* following reflection from the ball.

where

$$\begin{aligned} h_i^2 &= |(\sin\theta - y_0)\,\underline{\mathrm{i}}, (\cos\theta - D)|^2 \\ &= 1 + D^2 + y_0^2 - 2D\cos\theta - 2y_0\sin\theta \\ &= h^2 + y_0^2 - 2y_0\sin\theta. \end{aligned}$$

Using the law of reflection, i.e., $-\hat{\mathbf{t}}_i \cdot \hat{\mathbf{n}} = \hat{\mathbf{n}} \cdot \hat{\mathbf{t}}_e$, we find

$$\frac{D\cos\theta + y_o\sin\theta - 1}{h_i} = \frac{D\cos\theta - 1}{h},$$

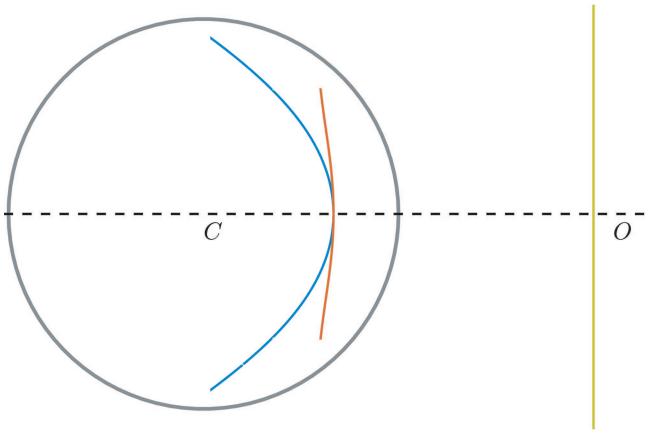


**FIG. 8.** Cross sections of *R*- and *A*-viewable surfaces (red, resp. blue) for a planar object placed normal to the axis at $D = 2R$ and viewed through a small hole at its center.

from which it follows that

$$y_0 = \frac{2D\sin\theta\,(D\cos\theta - 1)}{(D\cos 2\theta - \cos\theta)}. \tag{11}$$

The vanishing of the denominator, resulting in $y_0 \to \infty$, is equivalent to the incoming ray being normal to the symmetry axis.

### A. The *R*-viewable surface

The *R*-viewable surface containing points of radial focus is, as in Sec. III, computed using the one-dimensional set of rays emanating from *P* that are in the plane of Fig. 7. Consider a ray reflecting from $\hat{\mathbf{n}}' = \left[\sin(\theta+\varepsilon)\underline{i},\ \cos(\theta+\varepsilon)\right]$. The direction of the incoming ray is

$$\hat{\mathbf{t}}_i' = \frac{1}{h_i'}\left[(\sin(\theta+\varepsilon) - y_0)\,\underline{\mathrm{i}},\ (\cos(\theta+\varepsilon) - D)\right], \tag{12}$$

with

$$h_i'^2 = 1 + D^2 + y_0^2 - 2D\cos(\theta+\varepsilon) - 2y_0\sin(\theta+\varepsilon),$$

and hence,

$$h_i'\left.\frac{\partial h_i'}{\partial\varepsilon}\right|_{\varepsilon=0} = D\sin\theta - y_0\cos\theta. \tag{13}$$

From (9), the direction of the reflected ray is

$$\begin{aligned} \hat{\mathbf{t}}_e' = \frac{1}{h_i'}\big[&(-\sin(\theta+\varepsilon) + D\sin 2(\theta+\varepsilon) - y_0\cos 2(\theta+\varepsilon))\,\underline{\mathrm{i}}, \\ &\times (-\cos(\theta+\varepsilon) + D\cos 2(\theta+\varepsilon) + y_0\sin 2(\theta+\varepsilon))\big], \end{aligned}$$

and hence,

$$\begin{aligned} \left.\frac{\partial\hat{\mathbf{t}}_e'}{\partial\varepsilon}\right|_{\varepsilon=0} = \frac{1}{h_i}\big[&(-\cos\theta + 2D\cos 2\theta + 2y_0\sin 2\theta)\,\underline{\mathrm{i}}, \\ &\times (\sin\theta - 2D\sin 2\theta + 2y_0\cos 2\theta)\big] \\ &- \frac{1}{h_i^3}(D\sin\theta - y_0\cos\theta)\cdot\hat{\mathbf{t}}_e'|_{\varepsilon=0}. \end{aligned}$$

To compute the viewable surface, note as before that the reflected ray can be parameterized as $\mathbf{r}_R = \hat{\mathbf{n}}' + s\hat{\mathbf{t}}_e'$ and that on the viewable surface

$$\mathrm{d}\mathbf{r}_R = \left.\frac{\partial\hat{\mathbf{n}}'}{\partial\varepsilon}\right|_{\varepsilon=0}\mathrm{d}\varepsilon + \hat{\mathbf{t}}_e'|_{\varepsilon=0}\,\mathrm{d}s + s\left.\frac{\partial\hat{\mathbf{t}}_e'}{\partial\varepsilon}\right|_{\varepsilon=0}\mathrm{d}\varepsilon = 0,$$

from which it follows that the location on the surface is

$$s_R = \frac{h_i(D\cos\theta - 1)}{(3D\cos\theta - 1 + 2y_0\sin\theta - 2D^2\cos 2\theta - 2y_0 D\sin 2\theta)}.$$

The coordinates $y_R$ and $z_R$ on the viewable surface are found to be

$$\begin{aligned} z_R &= \cos\theta + s_R\frac{(D - \cos\theta)}{h}, \\ y_R &= \sin\theta - s_R\frac{\sin\theta}{h}. \end{aligned} \tag{14}$$

The cross section of the *R*-viewable surface for a planar object placed a distance $2R$ in front of the witch ball is shown in red in Fig. 8.

Although it is nearly flat, the surface fails to have a vanishing second derivative for any $D$.

### B. The $A$-viewable surface

To compute the $A$-viewable surface, we need the focus of a rays emanating from $P$ normal to the plane of Fig. 7, consider a ray with a differential orientation $\eta$. The incident direction, point of reflection, and other relevant quantities are

$$\hat{\mathbf{n}}' = \left[\sin\theta\ \underline{\mathrm{i}\,\mathrm{e}^{i\eta}},\ \cos\theta\right],$$

$$\hat{\mathbf{t}}_i' = \frac{1}{h_i'}\left[\sin\theta\ \underline{\mathrm{i}\,\mathrm{e}^{i\eta}} - y_0\,\underline{\mathrm{i}},\ \cos\theta - D\right],$$

$$h_i'^2 = D^2 + y_0^2 + 1 - 2D\cos\theta - 2y_0\sin\theta\cos\eta,$$

$$\frac{\partial h_i'}{\partial\eta}\Big|_{\eta=0} = 0,$$

$$\hat{\mathbf{t}}_e'\big|_{\eta=0} = \frac{1}{h_i}\left[(-\sin\theta - y_0\cos 2\theta + D\sin 2\theta)\,\underline{\mathrm{i}}\right.$$
$$\left.\times\,(-\cos\theta + y + 0\sin 2\theta + D\cos 2\theta)\right],$$

$$\frac{\partial\hat{\mathbf{t}}_e'}{\partial\eta}\Big|_{\eta=0} = \frac{1}{h_i}(-\sin\theta - 2y_0\sin^2\theta - D\sin 2\theta)\left[\underline{1},\ 0\right].$$

The reflected ray, parameterized, is $r_A = \mathbf{n}' + s\mathbf{t}_e'$, and the location on the viewable surface corresponds to

$$s_A = -\frac{h_i}{(2D\cos\theta + 2y_0\sin\theta - 1)},$$

and consequently,

$$z_A = \cos\theta + s_A\frac{(D - \cos\theta)}{h},$$
$$y_A = \sin\theta - s_A\frac{\sin\theta}{h}. \tag{15}$$

The cross section of the $A$-viewable surface is shown in blue in Fig. 8.

In Sec. V, we experimentally demonstrate the existence of two distinct images along a viewing direction and validate the expressions (14) and (15).

## V. EXPERIMENTAL VALIDATION

Typical witch balls are not sufficiently smooth to test the calculations outlined in Sec. IV. Experiment validation was conducted using the arrangement shown schematically in Fig. 9. The mirror is an optical quality convex spherical mirror with a radius of curvature $R = 20.0$ cm, a focal length of $f = -10.0$ cm, a diameter of 50.0 mm, and a protected aluminum coating. The center of the sphere is $C$. The object at $P$ is a cross with vertical and horizontal line segments of length 6 cm and width 2 mm. Images are recorded using a Scion camera with a *ccd* chip of 1200 × 1600 pixels with pixel spacing 4.0 $\mu$m. A Navitar Zoom 7000 18-108 mm macro lens is used to focus the reflected object onto the detector. Camera positioning was accomplished using translation stages having micrometer drives with a spatial resolution of 10 $\mu$m. The configuration shown lies in a horizontal plane.

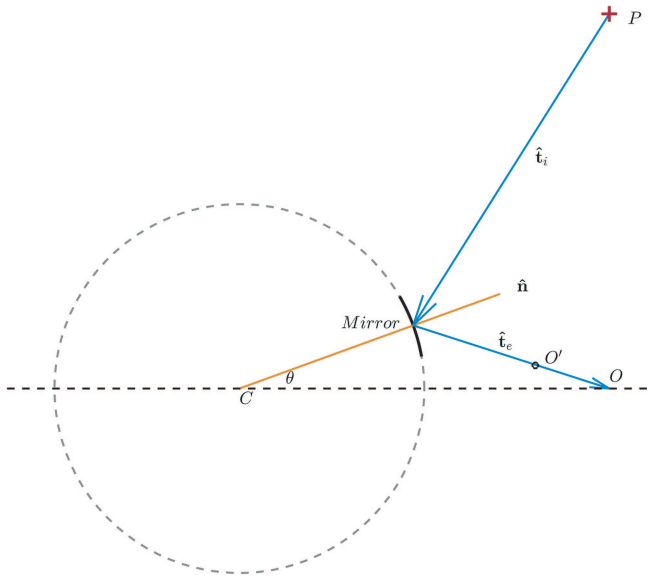


**FIG. 9.** A schematic of the experiment. The mirror, shown by a solid line, is a section of a hypothetical witch ball centered at $C$, which is marked by a dashed line. A cross of vertical and horizontal lines at $P$ is viewed through the camera at $O$. The camera can be moved along $OO'$, the direction of the emergent ray.

The mirror and the witch ball from which it is assumed to be cleaved are shown in solid and dashed lines, respectively. The mirror axis is held in place, and each setting is initiated by a pre-specified rotation of the mirror. The center of the sphere, $C$, is identified using the radius of curvature; the camera is placed on the symmetry axis a distance $D = 65$ mm from $C$. The object $P$ is moved in the plane normal to the symmetry axis until its image is at the focal plane of the mirror. The azimuthal line (i.e., vertical line in our setup) is set in focus, as confirmed using the intensity profile of the cross section; see Fig. 10(c). The best focus is defined by minimizing the half-width of the intensity curve shown in Fig. 10(c). Typically, this optimal focus remains unchanged when $O$ is moved by ≈1–2 mm; these distances give an estimate of the measurement error. Generally, the image of the radial (horizontal) line is not in focus at this point as seen in Fig. 10(c).

Refocusing the camera to locate the second image will change the focal plane in a way that is difficult to estimate. Instead, we search for the second image by moving the camera forward, say, by a distance $\delta$, along the direction $-\hat{\mathbf{t}}_e$ of the exit ray while maintaining the same focus. It is found that the horizontal line of the object focuses when the camera has moved to a point $O'$; $\delta = |OO'|$. The use of the micrometer permits the estimation of $\delta$ to within 10 $\mu$m, if necessary. Generally, the focus of the azimuthal line is lost at this point as seen from Fig. 10(d). The views at $O$ and $O'$, shown in Fig. 10, clearly illustrate the existence of two distinct images.

Since the camera has moved during the experiment, $\delta$ is not the distance between the $R$ and $A$ viewable surfaces with fixed viewing at $O$. The location of azimuthal focus, $\mathbf{r}_R(D,\theta)$, is given by (14), while that at radial focus needs to be calculated for viewing at $O'$. To do

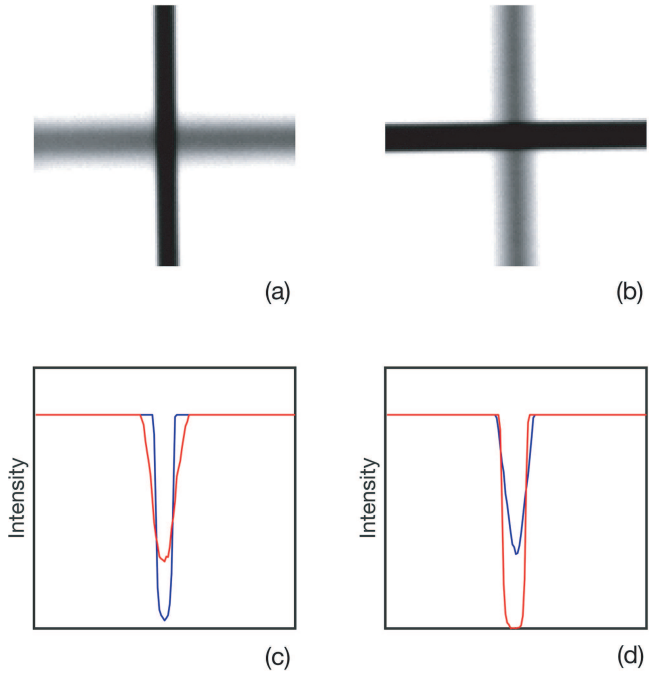


**FIG. 10.** The two images with (a) a sharp focus on the azimuthal (vertical) line and (b) a sharp focus on the radial (horizontal) line. The variation in the intensity for the two images is shown in (c) and (d). The red (resp. blue) lines show the intensity profile for the radial (resp. azimuthal) lines. Observe that the focused images have a higher value for the peak intensity gradient.

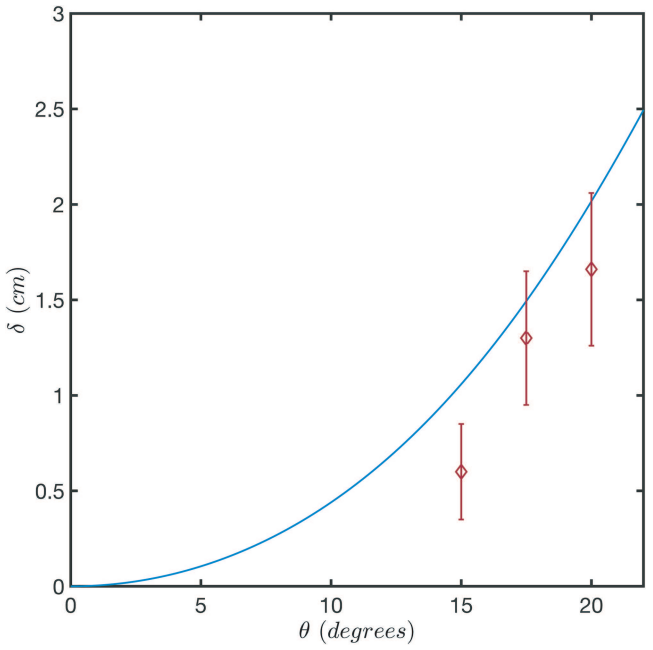


**FIG. 11.** The solid line shows the inclination of the mirror vs $\delta$, the camera movement to get from the image with vertical focus to that with horizontal focus. The diamonds show the best estimate of $\delta$, and the error bars represent distances over which the width of the intensity remains unchanged.

so, we note first that the angle $\psi$ between the exit ray $\mathbf{t}_e$ and $CO$ is small in our experiments. In addition, $\delta \ll D$, and hence, distance $D' \equiv |CO'| \approx D - \delta$. The angle subtended by $OO'$ at $C$ is, by the law of sines, $\delta\theta = \sin^{-1}(\delta \sin\psi/D')$. Hence, the angle $\theta'$ between $CO'$ and $\hat{\mathbf{n}}$ is $\theta' = \theta + \mathcal{O}(\psi^2, \psi\delta, \delta^2)$; i.e., it is unchanged to first order in $\delta$ and $\psi$. The location $\mathbf{r}_A(D', \theta')$ of the horizontal focus with the camera at $O'$ can be calculated to first order in perturbation in $\delta$ and $\psi$. The value of $\delta$ can then be obtained by solving

$$\delta = |\mathbf{r}_R(D, \theta) - \mathbf{r}_A(D', \theta')|.$$

The solid line in Fig. 11 shows $\delta$ as a function of $\theta$.

The experimental values of $\delta$ for $\theta = 15^\circ$, $17.5^\circ$, and $20^\circ$ are shown with the error bars originating from our inability to precisely locate the point of best focus.

## VI. DISCUSSION

Locations of optical images are typically calculated using ray diagrams or by maximizing the flux density of emergent rays (Fock, 1965 and Keller and Streifer, 1971). The critical role of caustics in image formation was discussed in Born and Wolf (1965), Shealy (1976), Nussenzveig (1977), Nye (1999), Berry (2015), and Berry (2021). Feigenbaum (unpublished) highlighted that, following passage through a general optical system, a wavefront does not appear to emerge from a single point. On the contrary, it is a Gaussian surface with partial focus along two principal directions; the corresponding centers of curvature were referred to as "non-objects." Thus, a viewer will observe two distinct images of a point source, and it was observed by Feigenbaum that our visual system preferentially focuses on the one with (or close to) vertical astigmatism. In viewing an extended object, the two sets of images span two surfaces, referred to as viewable surfaces. In general, these viewable surfaces are not the tangential surfaces (where adjacent rays in the meridional plane, i.e., plane containing the mirror axis and the object, pass through) and sagittal surfaces (where adjacent rays normal to the meridional plane pass through) discussed in the context of image formation in axisymmetric optical configurations (Avendaño Alejo *et al.*, 2019). The latter are computed through ray diagrams in two orthogonal planes. Anamorphic images and the corresponding viewable surfaces were calculated in Feigenbaum (unpublished). Imaging of underwater objects was discussed in Horváth *et al.* (2003), Eckmann (2021), and Feigenbaum (unpublished).

The goal of our work was to compute images and viewable surfaces in reflections from a spherical mirror. We computed them for three configurations, the first of which was for an incoming parallel beam of light (Berry, 1972; 2015). The two images and the corresponding viewable surface contained points of radial and azimuthal focus. The surface of radial focus was azimuthally symmetric with a cusp singularity on the symmetry axis. The surface of azimuthal focus degenerated to a one-dimensional subset of the symmetry axis. Both viewable surfaces for the next two configurations were non-degenerate. In one, we calculated viewable surfaces

for an observer at a distance $D$ viewing infinitely distant objects. We found that the surface of radial focus was planar to fourth order when $D = (2 + \sqrt{3})R$. The final example involved viewing of a planar object through an opening at its intersection with a radius of the sphere normal to the plane. Several predictions were experimentally validated.

The two viewable surfaces in all configurations we study have the following feature: one surface consisted of points of radial focus and the other points of azimuthal focus. The preferential focus for our visual system is for points of horizontal focus or vertical astigmatism. This leads to an interesting question on viewing a plane in the configuration shown in Fig. 7. The viewable surfaces, shown in Fig. 8, contain points of radial (red) and azimuthal (blue) focus. The first viewable surface can easily be captured by a camera. What will a subject observe in viewing the image in the mirror? Will they see the surface of radial focus at the upper and lower locations and the surface of azimuthal focus at the sides? Alternatively, will our ability to reconstruct local scenes using global properties (Greene and Oliva, 2009) allow a subject to focus on one of the two images? We expect to conduct a study to address this issue.

## DEDICATION

The work reported here was inspired by studies of Mitchell J. Feigenbaum and insightful discussions with him. We dedicate this work to his memory.

## ACKNOWLEDGMENTS

J.-P.E. was partially supported by the Fonds National Suisse Swissmap.

## AUTHOR DECLARATIONS

### Conflict of Interest

The authors have no conflicts to disclose.

### Author Contributions

**Jean-Pierre Eckmann:** Formal analysis (equal); Investigation (equal); Methodology (equal); Writing – original draft (equal); Writing – review & editing (equal). **Gemunu H. Gunaratne:** Formal analysis (equal); Investigation (lead); Methodology (equal); Writing – original draft (equal); Writing – review & editing (equal). **Jason Shulman:** Investigation (supporting); Methodology (equal); Writing – original draft (supporting); Writing – review & editing (supporting). **Lowell T. Wood:** Investigation (equal); Methodology (equal); Writing – original draft (supporting); Writing – review & editing (supporting).

## DATA AVAILABILITY

The data that support the findings of this study are available from the corresponding author upon reasonable request.

## REFERENCES

Avendaño Alejo, M., "Caustics in a meridional plane produced by plano-convex aspheric lenses," J. Opt. Soc. Am. A **30**(3), 501–508 (2013).
Avendaño Alejo, M., Roman-Hernandez, E., Castillo-Santiago, G., DelOlmo-Marquez, J., and Casteñeda, L., "Sagittal and tangential foci produced by tilted plane wavefronts through simple lenses," Appl. Opt. **58**(22), 5959–5967 (2019).
Bartlett, A. A., Lucero, R., and Johnson, G. O., "Note on a common virtual image," Am. J. Phys. **52**, 640–643 (1984).
Berry, M. V., "Reflections on a Christmas-tree bauble," Phys. Educ. **7**, 1–6 (1972).
Berry, M. V., "The squint moon and witch ball," New J. Phys. **17**, 060201 (2015).
Berry, M. V., "Distorted mirror images organized by cuspoid and umbilic caustics," J. Opt. **23**, 125402 (2021).
Born, M. and Wolf, E., *Principles of Optics* (Pergamon, New York, 1965).
Eckmann, J.-P., "Broken pencils and moving rulers: After an unpublished book by Mitchell Feigenbaum," Am. J. Phys. **89**, 955–962 (2021).
Feigenbaum, M. J., *Reflections on a Tube*, edited by J.-P. Eckmann (unpublished).
Fock, V. A., *Electromagnetic Diffraction and Propagation Problems* (Pergamon, New York, 1965).
Greene, M. A. and Oliva, A., "Recognition of natural scenes from global properties: Seeing the forest without representing the trees," Cognit. Psychol. **58**, 137–176 (2009).
Horváth, G., Buchta, K., and Varjú, D., "Looking into the water with oblique head tilting: Revision of the aerial binocular imaging of underwater objects," J. Opt. Soc. Am. **20**, 1120–1131 (2003).
Keller, J. B. and Streifer, W., "Complex rays with an application to Gaussian beams," J. Opt. Soc. Am. **61**, 40–43 (1971).
Kinsler, L. E., "Imaging of underwater objects," Am. J. Phys. **13**, 255–257 (1945).
Nussenzveig, H. M., "The theory of the rainbow," Sci. Am. **236**, 116–127 (1977).
Nye, J. F., *Natural Focusing and Fine Structure of Light: Caustics and Wave Dislocations* (Institute of Physics Publishing, 1999).
Shealy, D. L., "Analytical illuminance and caustic surface calculation in geometrical optics," Appl. Opt. **15**, 2588–2596 (1976).